

Language Driven Occupancy Prediction

Zhu Yu¹ Bowen Pang¹ Lizhe Liu^{2*} Runmin Zhang¹ Qihao Peng²
Maochun Luo² Sheng Yang² Mingxia Chen² Si-Yuan Cao¹ Hui-Liang Shen^{1*}

¹Zhejiang University ²Autonomous Driving Lab, Cainiao Network

<https://github.com/pkqbajng/LOcc>

Abstract

We introduce **LOcc**, an effective and generalizable framework for open-vocabulary occupancy (OVO) prediction. Previous approaches typically supervise the networks through coarse voxel-to-text correspondences via image features as intermediates or noisy and sparse correspondences from voxel-based model-view projections. To alleviate the inaccurate supervision, we propose a **semantic transitive labeling** pipeline to generate dense and fine-grained 3D language occupancy ground truth. Our pipeline presents a feasible way to dig into the valuable semantic information of images, transferring text labels from images to LiDAR point clouds and ultimately to voxels, to establish precise voxel-to-text correspondences. By replacing the original prediction head of supervised occupancy models with a geometry head for binary occupancy states and a language head for language features, **LOcc** effectively uses the generated language ground truth to guide the learning of 3D language volume. Through extensive experiments, we demonstrate that our semantic transitive labeling pipeline can produce more accurate pseudo-labeled ground truth, diminishing labor-intensive human annotations. Additionally, we validate **LOcc** across various architectures, where all models consistently outperform state-of-the-art zero-shot occupancy prediction approaches on the *Occ3D-nuScenes* dataset. Notably, even based on the simpler *BEVDet* model, with an input resolution of 256×704 , **LOcc-BEVDet** achieves an *mIoU* of 20.29, surpassing previous approaches that rely on temporal images, higher-resolution inputs, or larger backbone networks. The code for the proposed method is available.

1. Introduction

Vision-based occupancy prediction aims to estimate both the complete scene geometry and semantics using only image inputs, which serves as a critical foundation for various

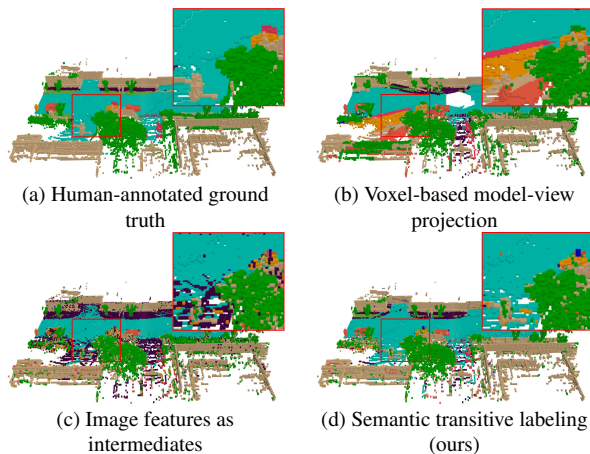


Figure 1. **Comparison of Pseudo-Labeled 3D Language Occupancy Ground Truth From Different Pipelines.** Human-annotated ground truth requires substantial human effort. Voxel-based model-view projection (b) often introduces labeling errors for occluded voxels, while using image features as intermediates (c) leads to coarse voxel-to-text correspondences. In contrast, our semantic transitive labeling pipeline (d) presents a feasible way to dig into the valuable semantic information of images, transferring texts from images to LiDAR point clouds and ultimately to voxels, producing dense and fine-grained 3D language occupancy ground truth, diminishing laborious human annotations.

3D perception tasks, such as autonomous driving [10, 20], embodied agent [33], mapping and planning [38]. Existing supervised occupancy prediction approaches [24, 30, 31, 34, 36] are generally constrained to predicting a fixed set of semantic categories, as the dense occupancy ground truth is generated by merging multi-frame LiDAR point clouds with semantic annotations. In this process, human annotators must label each point across thousands of LiDAR frames with a semantic class, which remains highly labor-intensive and costly. Instead, open-vocabulary occupancy (OVO) facilitates predicting the occupancy with arbitrary sets of vocabularies using only unlabeled image-LiDAR data for training [32, 47].

*Corresponding author.

Due to the lack of large-scale 3D occupancy datasets with language annotations, distilling knowledge from vision-language models [4, 17, 28, 32, 47] into the occupancy prediction network presents a viable solution. However, the performance of such approaches remains suboptimal, and often demands much computational cost.

To address these issues, we revisit two core aspects for OVO: label transferring process to bridge the gap between language and 3D data, and reconstruction process to assign each voxel a text label. For the label transferring process, using image features from the pretrained vision-language models as intermediates [4, 32] and aligning 3D features with them is a straightforward way to establish indirect correspondences between 3D data and texts. Nevertheless, these vision-language approaches force the vision encoder to align with scene- or region-level texts [28] or produce low-resolution feature maps [40], which lack precise guidance required for pixel-level understanding, resulting coarse voxel-to-text correspondences. Regarding the reconstruction process, previous approaches [32, 47] generally treat all the voxels as surface ones, and project them onto current frames to obtain 3D semantic pseudo labels. But this voxel-based model-view projection overlooks the occlusion problem, leading to noisy and sparse voxel-to-text correspondences.

In this work, we propose a **semantic transitive labeling** pipeline to generate dense and fine-grained 3D language occupancy ground truth, relieving laborious procedures. In the label transferring process, we use large vision-language models (LVLN)[1, 2, 21] and open-vocabulary segmentation models (OV-Seg)[8, 39, 40] to assign text labels to each pixel, producing high-resolution segmentation maps. Then, through the projection of LiDAR points, the text labels are transferred to the LiDAR points, bridging the gap between 3D data and texts. In the reconstruction process, we model the occlusion relationships of the point clouds during the projection, preventing the wrong label assignment of voxel-based model-view projection. With the pseudo-labeled LiDAR data, we reconstruct a temporally dense scene by merging multi-frame LiDAR points to obtain a dense 3D spatial representation. Furthermore, to reduce the impact of segmentation noise from individual frames, we apply majority-voting voxelization to assign the most frequent label to each voxel. The resulting ground truth enhances 3D language supervision for open-vocabulary occupancy networks, as illustrated in Fig. 1.

Based on the semantic transitive labeling pipeline, we devise **LOcc**, an effective and generalizable framework that is compatible with most existing supervised occupancy models [11, 12, 20] for OVO. This is accomplished by replacing the original prediction head with a geometry head to predict binary occupancy states and a language head to estimate language features. To efficiently align high-

dimensional CLIP [28] embeddings, we devise a language autoencoder that maps them to a low-dimensional latent space, reducing computational cost. We validate our framework on several mainstream approaches, referred to as LOcc-BEVFormer, LOcc-BEVDet, and LOcc-BEVDet4D. All three models consistently surpasses all the previous state-of-the-art zero-shot occupancy prediction approaches on the Occ3D-nuScenes dataset. Notably, even the simpler LOcc-BEVDet, with an input resolution of 256×704 , achieves an mIoU of 20.29, outperforming previous methods that rely on temporal image inputs, higher-resolution inputs, or larger backbone networks. In summary, our contributions are summarized as follows:

- We propose LOcc, an effective and generalizable framework that is compatible with most existing supervised methods for OVO. To reduce the computational cost for the language feature alignment, a text-based autoencoder is introduced to map the high-dimensional CLIP embeddings to a low-dimensional latent space.
- We propose a semantic transitive labeling pipeline for generating dense and fine-grained 3D language occupancy ground truth. This pipeline ensures that text semantic labels can be effectively transferred from images to LiDAR point clouds and ultimately to voxels. We experimentally verify that our pipeline can produce more accurate pseudo-labeled ground truth, diminishing time-consuming human annotations.
- We validate our LOcc framework with several mainstream models, which all demonstrate superior performance over previous state-of-the-art methods, proving its generalizability and effectiveness.

2. Related Work

2.1. Vision-based Occupancy Prediction

Occupancy prediction jointly estimates the occupancy state and semantic label for every voxel in the scene using images. Voxels are classified as free, occupied, or unobserved, with occupied voxels assigned corresponding semantic labels. Early works [3, 6, 19, 43, 46, 48] typically use monocular or stereo images as inputs, also referred to as semantic scene completion (SSC). With advancements in 3D perception [11, 12, 20], the occupancy of surrounding scenes using multi-camera images [13, 23, 37, 42] has garnered significant attention due to its strong representation capabilities in 3D space. SurroundOcc [36] introduces a new pipeline for constructing dense occupancy ground truth. Occ3D [30] establishes benchmarks for surround occupancy prediction through a three-stage data generation pipeline: voxel densification, occlusion reasoning, and image-guided voxel refinement. OpenOccupancy [34] provides a benchmark with higher-resolution ground truth, while OccNet [31] offers flow annotations.

Although the above approaches provide an automatic data generation pipeline to construct dense occupancy ground truth, they require LiDAR data with semantic annotations. To achieve this, human annotators must label each point across thousands of LiDAR frames with a semantic class, which remains highly labor-intensive and costly. Besides, the valuable semantic information of images are ignored during the occupancy generation process. Instead, in this work, we propose a semantic transitive labeling pipeline to dig into the valuable semantic information from images, transferring text labels from images to LiDAR point clouds and ultimately to voxels. It is compact and does not require labor-intensive human annotations, offering a more cost-effective way to incorporate semantic information from images.

2.2. Open-Vocabulary Understanding

The recent advances of vision-language models [28] have showed a remarkable zero-shot performance by using only paired images and captions for model training, demonstrating the strong connection between images and natural language. Then, numerous works explore the potential of language driven downstream applications, such as object detection [7, 44], tracking [18], and segmentation [8, 17, 39, 40]. Taking the image features of these 2D foundation models as intermediaries, OpenScene [25] distills 2D vision-language knowledge into a 3D point cloud network and achieve zero-shot 3D segmentation. LERF [15] is the first to embed CLIP features into NeRF for controllable rendering. LangSplat [27] uses SAM [16] to tackle the point ambiguity issue for 3D language field modeling.

2.3. Open-Vocabulary Occupancy Prediction

Benefiting from the development of vision-language foundation models, OVO enables the prediction of occupancy associated with arbitrary vocabulary sets without requiring manual annotations of extensive 3D voxel data. POP-3D [32] employs only unlabeled images and sparse LiDAR point clouds for training. It distills vision-language knowledge from the pretrained LSeg [17] into the occupancy networks by computing cosine similarity between 3D features and their corresponding 2D features, obtained by projecting the point cloud onto the image plane. VEON [47] introduces a side adaptor network to integrate CLIP [28] into the occupancy prediction model. However, the feature maps from existing vision-language models lack the fine-grained guidance required for pixel-level understanding, failing to establish precise correspondences between voxels and texts. Furthermore, current works typically treat all the voxels as surface ones and employ voxel-based model-view projection to obtain supervision, leading to a lots of misprojections.

3. Method

Our proposed LOcc framework mainly consists of two aspects: generating dense and fine-grained pseudo-labeled 3D language occupancy ground truth, diminishing laborious human annotations (Sec. 3.1), and using the generated ground truth to train the OVO networks (Sec. 3.2). To reduce computational cost, an autoencoder is introduced to map the CLIP [28] embeddings into a lower dimensional latent space (Sec. 3.3).

3.1. Pseudo-Labeled Ground Truth Generation

We propose a semantic transitive labeling pipeline to generate dense and fine-grained 3D language ground truth. The overview framework is illustrated in Fig. 2. Specifically, we first use vision-language foundation models, including Large Vision-Language Model (LVLM) and Open-Vocabulary Segmentation Model (OV-Seg), to associate each pixel with a text-based pseudo label. We then project the unlabeled LiDAR point clouds onto the image plane to propagate these pseudo labels to each point. The resultant pseudo-labeled LiDAR point clouds can further be used for scene reconstruction. Each voxel subsequently derives its pseudo label from the pseudo-labeled LiDAR points it contains, ultimately generating dense and fine-grained pseudo-labeled language occupancy ground truth.

Vocabulary Extraction with LVLM. Benefiting from the advent of LVLMs [1, 21], we can decode visual information in images using textual descriptions. Here, we employ the LVLM as an initial perception model to list the objects within each image. Fig. 3 illustrates the process of requiring the LVLM to list all classes within an image using Qwen-VL[2]. The conversation process follows the chain-of-thought [35] approach. Specifically, rather than directly requesting the LVLM to generate class nouns, we first ask it to provide a description of the scene, followed by a dialogue in which we prompt the LVLM to list the names of all identified classes. To enhance the LVLM’s understanding of outdoor environments, we provide an example in advance to assist this process when analyzing a large number of cases. The results extracted from single-frame surround images are then consolidated to represent the overall classes for that frame.

Pixel-to-Text Association with OV-Seg. Having obtained the vocabularies within a frame of surround images, we can establish pixel-to-text association with open-vocabulary semantic segmentation models [8, 39, 40]. This process begins by mapping the image and vocabularies into a shared feature space via the feature-aligned vision encoder Φ_I and text encoder Φ_T , respectively. Each pixel is then assigned a text label by computing cosine similarity with the set of vocabulary embeddings, with the highest-scoring text designated as the label for that pixel. Specifically, for the k -th frame surround-view im-

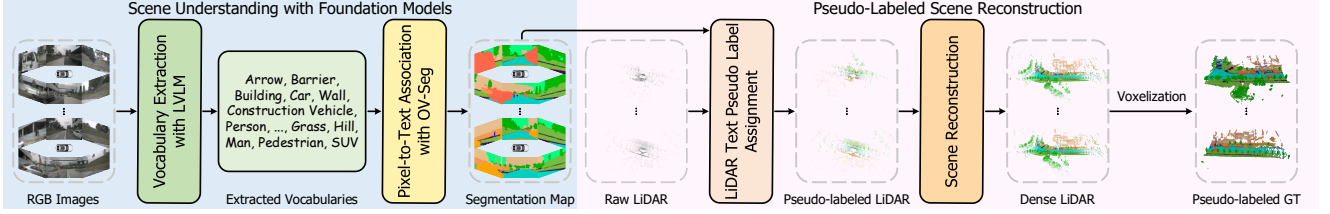


Figure 2. Framework of our semantic transitive labeling pipeline for generating dense and fine-grained pseudo-labeled 3D language occupancy ground truth. Given surround images of the entire scene, we first map them to a vocabulary set using a large vision-language model (LVLm) and associate pixels with these terms through an open-vocabulary segmentation model (OV-Seg). Based on the segmentation results, we assign pseudo labels to the points by projecting them onto the corresponding image plane and merge all the point clouds to form a complete scene. Finally, we voxelize the scene reconstruction results to establish dense and fine-grained voxel-to-text correspondences, generating the pseudo-labeled ground truth.

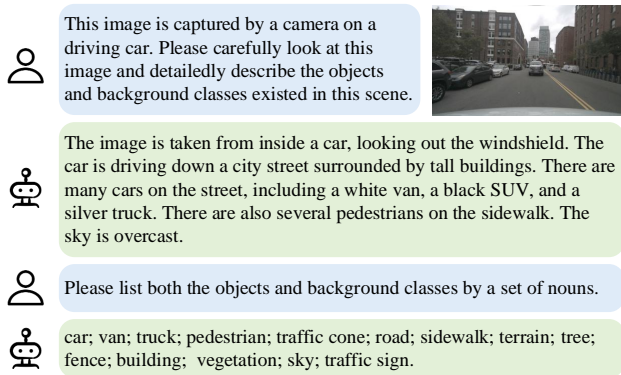


Figure 3. An example of the conversation process with Qwen-VL [2] to extract vocabularies from an individual image.

ages $\mathcal{I}_k = \{\mathbf{I}_{i,k} \in \mathbb{R}^{H \times W \times 3}, i \in \{1, \dots, N_c\}\}$ and vocabularies $\mathcal{T}_k = \{\mathbf{T}_{j,k}, j \in \{1, \dots, N_{t,k}\}\}$, their corresponding segmentation maps $\mathcal{S}_k = \{\mathbf{S}_{i,k} \in \mathbb{R}^{H \times W}, i \in \{1, \dots, N_c\}\}$ can be obtained as

$$\mathbf{F}_{i,k} = \Phi_I(\mathbf{I}_{i,k}) \in \mathbb{R}^{H \times W \times C}, \mathbf{E}_{j,k} = \Phi_T(\mathbf{T}_{j,k}) \in \mathbb{R}^C, \\ \mathbf{S}_{i,k}(x, y) = \arg \max_{\mathbf{T}_{j,k}} \cos(\mathbf{F}_{i,k}(x, y), \mathbf{E}_{j,k}), \quad (1)$$

where \mathbf{F}_i represents the feature maps of images and \mathbf{E}_j represents the embeddings of texts. Here, $N_{t,k}$ indicates the length of the vocabulary set for the k -th frame. Typically, Φ_I generates feature maps at a lower resolution and the final high-resolution segmentation maps are produced using an upsampling decoder [8]. For simplicity, we let \mathbf{F}_i have the same resolution with the original image.

In our investigation, we found that the LVLm occasionally fails, overlooking many important classes and listing only a limited vocabulary set within a single frame. To address this issue, we treat multiple frames as a unified sequence, integrating the vocabularies from each frame into a cohesive set $\mathcal{T} = \{\mathbf{T}_j, j \in \{1, \dots, N_t\}\}$, where $N_t = \sum_k N_{t,k}$. This integrated set is then used to perform open-

vocabulary segmentation as described in Eq. 1. The key motivation behind this approach is the overlap between consecutive frames, where recurring objects display a degree of similarity. Consequently, frames with incomplete text classes can be supplemented by the outputs from adjacent frames within the same sequence.

LiDAR Text Pseudo Label Assignment. Using the generated segmentation maps, we can assign text pseudo labels to the unlabeled LiDAR $\mathcal{P} = \{\mathbf{P}_k, k \in \{1, \dots, K\}\}$. Specifically, for a point $\mathbf{P}_k(p)$ in the k -th frame point cloud, its corresponding image coordinates on the N_c surround images are defined as

$$(x_i, y_i, z_i) = \mathbf{K}_i(\mathbf{R}_i \mathbf{P}_k(p) + \mathbf{t}_i), i \in \{1, \dots, N_c\}, \quad (2)$$

where $\mathbf{K}_i, \mathbf{R}_i, \mathbf{t}_i$ are camera intrinsic and extrinsic parameters. Among these coordinates, the one that lies within the image boundaries and has the smallest depth value z_i serves as the pixel corresponding to point $\mathbf{P}_k(p)$. This pixel is then used to sample the segmentation map to obtain the pseudo label $\hat{\mathbf{S}}(p)$ for $\mathbf{P}_k(p)$. This process can be summarized as

$$n = \arg \min_m z_m, 0 < x_m < W, 0 < y_m < H, \\ \hat{\mathbf{S}}(p) = \phi(\mathbf{S}_{n,k}, (x_n, y_n)), \quad (3)$$

where ϕ indicates the nearest neighbor sampling of $\mathbf{S}_{n,k}$ at the coordinate (x_n, y_n) .

Scene Reconstruction. The pseudo-labeled LiDAR data is then used to perform scene reconstruction to establish correspondences between the texts and the voxels. To combine the multi-frame point clouds, we first transform their coordinates into the world coordinate system using the calibration matrices and ego poses. For the k -th frame, we transform the unified point cloud to this frame and apply majority-voting voxelization on it to obtain the pseudo-labeled 3D language occupancy ground truth. Each voxel takes the most frequent text within it as its text label. Compare to the voxel-based model-view projection, our method obtains text label by projecting LiDAR point clouds onto

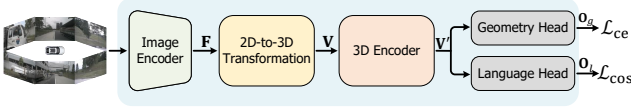


Figure 4. Overview of the open-vocabulary occupancy (OVO) model architecture.

image planes, which are easily calibrated with the corresponding images during the data collection process. Besides, the majority-voting is more robust and less susceptible to the influence of single-point projection errors, generating ground truth with higher metrics compared to the nearest-point voxelization, as shown in the ablation experiments.

3.2. Open Vocabulary Occupancy Prediction

Based on the processes described above, we successfully establish dense and fine-grained voxel-to-text correspondences. By minimally modifying most existing supervised occupancy methods [12, 12, 20], we can leverage the obtained pseudo-labeled 3D language occupancy ground truth to train a robust OVO model, without the need for additional complex network designs. The overall network architecture is shown in Fig. 4. Similar to most existing occupancy network structures, it involves an image encoder, a 2D-to-3D view transformation module, a 3D encoder, except the original prediction head is replaced by a geometry head to predict the binary occupancy state and a language head to estimate the language features.

Image Encoder. The image encoder includes an image backbone network for extracting multi-scale features, complemented by an FPN network to enhance features across different levels. The enhanced features $\mathbf{F} \in \mathbb{R}^{H \times W \times C}$ are then used to construct 3D features.

2D-to-3D Transformation. The 2D-to-3D view transformation aims to project multiview image features into the 3D voxel space. This can be achieved by either forward projection [26] or backward projection [20]. In this work, we verify the effectiveness of our proposed method on both projection approaches [11, 12, 20]. The constructed 3D volume \mathbf{V} has a shape of $X \times Y \times Z$ for voxel representation or $X \times Y$ when pooled into BEV representation

3D Encoder. After constructing the 3D volume \mathbf{V} , the 3D encoder further refines its representation by performing 3D convolution [9] or stacking self-attention layers [20] to obtain the fine-grained volume \mathbf{V}' . This refined volume \mathbf{V}' is then fed to a geometry head to estimate binary occupancy states \mathbf{O}_g and a language head to generate 3D language volume \mathbf{O}_l .

Training and Evaluation. During training, we jointly supervise the geometry and language heads to optimize the neural network. Given the binary occupancy ground truth

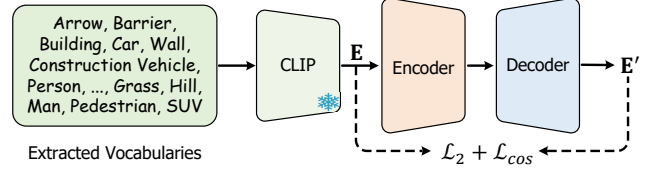


Figure 5. Framework of the autoencoder to map the language features into a low-dimensional latent space.

$\hat{\mathbf{O}}_g$, we adopt cross entropy loss to supervise \mathbf{O}_g ,

$$\mathcal{L}_{ce} = \text{CrossEntropy}(\hat{\mathbf{O}}_g, \mathbf{O}_g). \quad (4)$$

Given the pseudo-labeled 3D language ground truth, each voxel of it corresponds to a text. We perform alignment between \mathbf{O}_l and the CLIP embeddings of these texts $\hat{\mathbf{O}}_l$ using cosine similarity,

$$\mathcal{L}_{cos} = \sum_{p \in \mathcal{C}(\hat{\mathbf{O}}_g)} 1 - \cos(\hat{\mathbf{O}}_l(p), \mathbf{O}_l(p)), \quad (5)$$

where $\mathcal{C}(\hat{\mathbf{O}}_g)$ denotes the set of occupied voxels in $\hat{\mathbf{O}}_g$. The final loss function \mathcal{L} is a combination of \mathcal{L}_{ce} and \mathcal{L}_{cos} ,

$$\mathcal{L} = \mathcal{L}_{ce} + \mathcal{L}_{cos}. \quad (6)$$

During evaluation, \mathbf{O}_g first defines the set of occupied voxels. Then for each occupied voxel, its corresponding language feature is used to compute cosine similarity with the predefined text features, where the text with the highest score represents its semantics.

3.3. Language Autoencoder

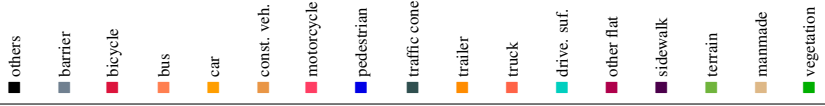
Generally, the dimension of CLIP features is 512. To reduce the memory requirements, we introduce a language autoencoder to map the language features into a low-dimensional latent space. The extracted vocabularies of the entire dataset contains approximately one thousand unique classes, allowing the autoencoder to be trained efficiently. Fig. 5 shows the framework of the autoencoder.

Specifically, given the vocabulary set $\mathcal{T}_a = \{\mathbf{T}_i, i \in 1, \dots, N_a\}$ of the entire dataset, the encoder Φ_E maps the D -dimensional CLIP features $\mathbf{E} \in \mathbb{R}^D$ to $\mathbf{E}' \in \mathbb{R}^{D'}$, where $D' < D$. Then we learn a decoder Φ_D to reconstruct the original embedding from the compressed \mathbf{E}' . The autoencoder is trained with a combination of L2 loss and cosine loss,

$$\mathcal{L}_a = \|\mathbf{E} - \hat{\mathbf{E}}\|_2 + \cos(\mathbf{E}, \hat{\mathbf{E}}), \quad (7)$$

where $\hat{\mathbf{E}}$ denotes the reconstructed embedding. After training the autoencoder, the language volume of the OVO model is aligned with the compressed embedding.

Table 1. 3D occupancy prediction performance on the Occ3D-nuScenes dataset. We report the mean IoU (mIoU) for semantics across different categories, along with per-class semantic IoUs. * represents the reproduced results in [42]. The methods marked with † indicate that they specifically design the set of vocabularies for training. The top three results among the methods supervised by pseudo-labeled ground truth are in red, green, and blue, respectively.

Model	Image Backbone	Image Size	mIoU																	
				others	barrier	bicycle	bus	car	const. veh.	motorcycle	pedestrian	traffic cone	trailer	truck	drive. suf.	other flat	sidewalk	terrain	manmade	vegetation
<i>Supervised by human-labeled ground truth.</i>																				
MonoScene [6]	ResNet-101	900 × 1600	6.06	1.75	7.23	4.26	4.93	9.38	5.67	3.98	3.01	5.90	4.45	7.17	14.91	6.32	7.92	7.43	1.01	7.65
OccFormer [46]	ResNet-101	900 × 1600	21.93	5.94	30.29	12.32	34.40	39.17	14.44	16.45	17.22	9.27	13.90	26.36	50.99	30.96	34.66	22.73	6.76	6.97
TPVFormer [13]	ResNet-101	900 × 1600	27.83	7.22	38.90	13.67	40.78	45.90	17.23	19.99	18.85	14.30	26.69	34.17	55.65	35.47	37.55	30.70	19.40	16.78
CTF-Occ [30]	ResNet-101	900 × 1600	28.5	8.09	39.33	20.56	38.29	42.24	16.93	24.52	22.72	21.05	22.98	31.11	53.33	33.84	37.98	33.23	20.79	18.0
BEVFormer wo TSA* [20]	ResNet-101	900 × 1600	38.05	9.11	45.68	22.61	46.19	52.97	20.27	26.5	26.8	26.21	32.29	37.58	80.5	40.6	49.93	52.48	41.59	35.51
BEVFormer* [20]	ResNet-101	900 × 1600	39.04	9.57	47.13	22.52	47.61	54.14	20.39	26.44	28.12	27.46	34.53	39.69	81.44	41.14	50.79	54.00	43.08	35.60
CVT-Occ* [42]	ResNet-101	900 × 1600	40.34	9.45	49.46	23.57	49.18	55.63	23.10	27.85	28.88	29.07	34.97	40.98	81.44	40.92	51.37	54.25	45.94	39.71
BEVDet [12]	ResNet-50	256 × 704	33.62	8.18	38.46	13.75	41.10	45.17	18.99	18.39	19.52	19.36	29.48	31.77	79.42	37.55	49.08	51.70	36.94	32.63
BEVDet4D [11]	ResNet-50	256 × 704	39.11	11.03	46.68	21.59	44.13	50.70	25.30	24.12	25.89	25.21	34.13	38.94	81.33	39.08	51.96	56.13	47.41	41.15
<i>Supervised by pseudo-labeled ground truth.</i>																				
SelfOcc (BEV) [14]	ResNet-50	384 × 800	6.76	0.00	0.00	0.00	9.82	0.00	0.00	0.00	0.00	0.00	6.97	47.03	0.00	18.75	16.58	11.93	3.81	
SelfOcc (TPV) [14]	ResNet-50	384 × 800	9.30	0.00	0.15	0.66	5.46	12.54	0.00	0.80	2.10	0.00	0.00	8.25	55.49	0.00	26.30	26.54	14.22	5.60
OccNeRF [45]	ResNet-101	928 × 1600	10.81	0.00	0.83	0.82	5.13	12.49	3.50	0.23	3.10	1.84	0.52	3.90	52.62	0.00	20.81	24.75	18.45	13.19
VEON-B† [47]	ViT-B	256 × 704	12.38	0.50	4.80	2.70	14.70	10.90	11.00	3.80	4.70	4.00	5.30	9.60	46.50	0.70	21.10	22.10	24.80	23.70
VEON-L† [47]	ViT-L	512 × 1408	15.14	0.90	10.40	6.20	17.7	12.7	8.50	7.60	6.50	5.50	8.20	11.80	54.50	0.40	25.50	30.20	25.40	25.40
LOcc-BEVFormer (ours)	ResNet-101	256 × 704	18.62	0.00	14.21	0.90	27.21	32.61	3.09	2.06	8.67	1.74	1.96	21.45	71.22	0.00	38.18	33.32	30.68	29.32
LOcc-BEVFormer (ours)	ResNet-101	512 × 1408	19.85	0.00	14.65	1.01	27.99	35.34	5.61	4.16	11.70	3.05	2.72	23.08	72.00	0.00	39.35	34.18	32.03	30.66
LOcc-BEVDet (ours)	ResNet-50	256 × 704	20.29	0.00	14.03	2.81	31.75	34.55	7.52	3.94	8.99	3.64	3.04	25.58	71.43	0.01	38.74	35.62	32.61	30.68
LOcc-BEVDet (ours)	ResNet-50	512 × 1408	20.84	0.00	13.85	3.28	31.85	37.09	8.22	4.84	10.78	3.24	2.47	26.95	72.35	0.00	39.58	35.29	33.35	31.23
LOcc-BEVDet4D (ours)	ResNet-50	256 × 704	22.95	0.00	15.01	5.76	29.86	38.90	11.61	4.61	13.46	6.99	2.64	30.69	73.61	0.00	40.38	39.16	38.80	38.68
LOcc-BEVDet4D (ours)	ResNet-50	512 × 1408	23.84	0.00	16.92	5.89	32.94	40.08	10.18	9.85	17.11	7.21	3.10	30.48	74.13	0.00	41.25	36.97	39.57	39.66

4. Experiments

4.1. Datasets and Metrics

Datasets. We evaluate LOcc on the nuScenes dataset [5, 30], a large-scale autonomous driving dataset collected across various cities and weather conditions. Each frame includes a LiDAR scan and six RGB images from different viewpoints. It contains 700 training scenes and 150 validation scenes. The spatial volume ranges from $-40m$ to $40m$ for the X and Y axes, and $-1m$ to $5.4m$ for the Z axis. Vox- elization of this volume produces a set of 3D grids with a resolution of $200 \times 200 \times 16$, where each voxel measures $0.4m \times 0.4m \times 0.4m$. The ground truth includes 17 unique labels (16 semantic classes and 1 free class).

Metrics. Following previous approaches [30], we list the intersection over union (IoU) and mean IoU (mIoU) metrics for occupied voxel grids and voxel-wise semantic predictions, respectively, providing a comprehensive analysis for geometry and semantic aspects of the scene.

4.2. Implementation Details

Network Structures. To demonstrate the generalizability of the proposed LOcc, we evaluate it on BEVFormer [20], BEVDet [12], and BEVDet4D [11], including both forward- and backward-projection methods. For BEVDet [12] and BEVDet4D [11], we employ ResNet-50 [9] as the image backbone. The resolution of the voxel features after the 2D-to-3D transformation is $200 \times 200 \times 16$, with a feature dimension of 64. For BEVFormer [20], we

adopt ResNet101-DCN [9] as the backbone, with the default size for BEV queries set to 200×200 , with a feature dimension of 256. We remove the temporal self-attention layer and use 6 cross-attention layers. For each query, it corresponds to 4 target points with different heights in 3D space, with height anchors uniformly predefined from $-1m$ to $5.4m$. The number of sampling points around each reference point is set to 8. For all models, the image size is resized to either 256×704 or 512×1408 , and the language features are compressed to a dimension of 128.

Training Setup. We implement the networks using PyTorch. The models are trained for 25 epochs on 8 NVIDIA 3090 GPUs, with a batch size of 1 on each GPU. We employ the AdamW [22] optimizer with $\beta_1 = 0.9, \beta_2 = 0.99$. The maximum learning rate is set to 3×10^{-4} , and the cosine annealing learning rate strategy is adopted for the learning rate decay, where the cosine warm up strategy is applied for the first 5% iterations.

4.3. Quantitative Results


We evaluate the effectiveness of the proposed LOcc framework on three models: BEVFormer [20], BEVDet [12] and BEVDet4D [11], referred to as LOcc-BEVFormer, LOcc-BEVDet, and LOcc-BEVDet4D, respectively.

We present the quantitative results of open-vocabulary occupancy prediction in Table 1. With the input image of size 256×704 , LOcc-BEVFormer, LOcc-BEVDet, and LOcc-BEVDet4D achieve an mIoU of 18.62, 20.29, and 22.95, respectively. Notably, LOcc-BEVDet, a more sim-

Table 2. Ablation study on the framework for generating dense and fine-grained pseudo-labeled 3D language occupancy ground truth. For label transferring process, we analyze three settings: (a) using image features from vision-language foundation models as intermediates, (b) using single-frame vocabularies, and (c) integrating vocabularies across multiple consecutive frames. For scene reconstruction process, we replace the majority-voting voxelization with (d) nearest-point voxelization and (e) voxel-based model-view projection. The best results for each model are in **red**.

Setting	Label Transferring Process			Scene Reconstruction Process			mIoU			
	Image Feat.	Single-frame vocab.	Consecutive-frame vocab.	Voting voxelization	Point-based Projection Nearest voxelization	Voxel-based Projection	LOcc-BEVFormer	LOcc-BEVDet	LOcc-BEVDet4D	
(a)	✓				✓		15.04	17.56	19.37	
(b)		✓			✓		17.87	19.61	22.15	
(c)			✓		✓		18.62	20.29	22.95	
(d)			✓			✓	18.32	19.98	22.68	
(e)			✓				✓	13.77	14.49	15.41

Table 3. Detailed metrics of the pseudo-labeled ground truth from different generation settings on the Occ3D-nuScenes dataset. The settings match those outlined in Table 2. We report the mean IoU (mIoU) for semantics across different categories. The top three results different settings are in **red**, **green**, and **blue**, respectively.

Setting	mIoU																	
		others	barrier	bicycle	bus	car	const. veh.	motorcycle	pedestrian	traffic cone	trailer	truck	drive. suf.	other flat	sidewalk	terrain	manmade	vegetation
(a)	22.12	0.00	10.20	7.18	29.59	35.22	15.70	12.80	11.19	1.86	15.28	21.56	58.52	0.00	25.80	22.72	55.53	52.92
(b)	22.66	0.00	8.07	4.51	23.33	37.48	9.62	11.42	14.04	10.50	4.61	19.86	60.30	0.24	30.94	25.97	59.17	65.22
(c)	25.53	0.00	9.40	8.47	30.16	38.00	11.43	20.20	11.39	11.54	9.55	25.73	61.86	0.40	36.41	33.00	59.42	67.10
(d)	23.80	0.00	8.90	6.75	27.86	34.21	10.19	15.75	10.05	8.68	8.83	22.67	60.91	0.50	34.91	31.82	56.91	65.70
(e)	19.55	0.00	7.19	4.28	24.62	21.15	8.30	8.43	6.71	4.63	8.65	16.01	55.41	0.50	26.32	31.01	50.95	58.22

pler model, surpasses all previous zero-shot and open-vocabulary approaches in terms of mIoU, even though many of these approaches use larger image backbones or higher-resolution inputs. Furthermore, when the image resolution is increased to 512×1408 , the models attain an better mIoU of 19.85, 20.84, and 23.84.

4.4. Ablation Study

We conduct ablation study to evaluate the effectiveness of the proposed LOcc framework.

Label Transferring Process. Table 2 shows an analysis of label transferring process. First, we replace the segmentation maps with image features from SAN [40], requiring the learned 3D features to align with these features, thereby indirectly establishing correspondences with texts. Setting (a) demonstrates that this model results in a performance drop across all models. Next, we apply our proposed hierarchical ground truth generation pipeline using single-frame vocabularies. As shown in setting (b), the model achieves mIoU scores of 17.87, 19.61, and 22.15, respectively. Finally, by treating multiple consecutive frames as a unified sequence and consolidating the vocabulary from each frame into a cohesive set for pseudo-label assignment, as indicated in setting (c), we observe additional performance gains, further validating the effectiveness of our voxel-to-language modeling approach.

Scene Reconstruction Process. Voxel-based model-view projection treats all the voxels as surface ones, over-

looking the occlusion problem and leading to noisy and sparse voxel-to-text correspondences. Instead, each frame of LiDAR is easily calibrated with corresponding images during the data collection process, with much less misprojections. Setting (e) demonstrates that using ground truth from voxel-based model-view projection to train the OVO models results in performance drops to 13.77, 14.49, and 15.41. In contrast, performing scene reconstruction with nearest-point voxelization yields notable improvements, as shown in setting (d). In contrast, majority-voting voxelization can bring better performance, where the mIoU is further improved to 18.62, 20.29, and 22.68 mIoU, as illustrated in setting (c). The results prove that majority-voting is more robust and less susceptible to the influence of single-point projection errors.

To further demonstrate the effectiveness of our transitive semantic labeling pipeline, we present detailed metrics for the pseudo-labeled ground truth generated under various settings in Table 3. Consistent with prior analyses, our pipeline with majority-voting voxelization, yields the highest-quality ground truth in terms of mIoU. Additionally, these results confirm that improvements in the generated pseudo-labeled ground truth directly enhance the performance of the final OVO model.

OV-Seg Models. Table 4 lists the metric values of the pseudo-labeled ground truth over the human-labeled ground truth using different OV-Seg models: SAN [40],

Table 4. Detailed metrics of the pseudo-labeled ground truth from different OV-Seg models on the Occ3D-nuScenes dataset. We report the mean IoU (mIoU) for semantics across different categories. The top three results among different methods are in **red**.

Method	mIoU	others	barrier	bicycle	bus	car	const. veh.	motorcycle	pedestrian	traffic cone	trailer	truck	drive. suf.	other flat	sidewalk	terrain	manmade	vegetation
		■	■	■	■	■	■	■	■	■	■	■	■	■	■	■	■	■
SAN [40]	25.53	0.00	9.40	8.47	30.16	38.00	11.43	20.20	11.39	11.54	9.55	25.73	61.86	0.40	36.41	33.00	59.42	67.10
ODISE [39]	25.80	0.00	11.45	7.83	37.66	38.10	6.94	22.74	16.28	0.52	5.58	24.59	63.09	0.27	37.16	34.12	62.72	69.47
CAT-Seg [8]	26.72	0.00	3.87	4.56	41.53	36.90	26.65	17.26	11.28	11.08	3.45	25.97	63.21	0.34	37.80	36.63	60.60	73.03

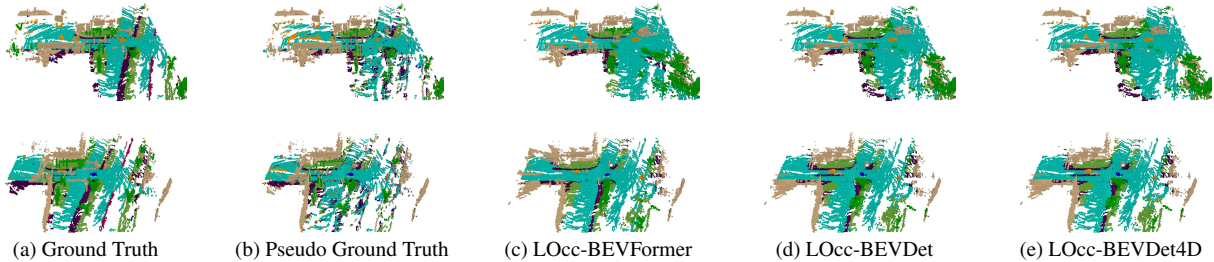


Figure 6. Quantitative visualization results on the Occ3D-nuScenes [30] dataset.

Table 5. Ablation study on the OV-Seg models.

Method	mIoU		
	LOcc-BEVDet	LOcc-BEVDet4D	LOcc-BEVFormer
ODISE [39]	20.17	22.52	18.69
CAT-Seg [8]	20.68	22.76	18.57
SAN [40]	20.29	22.68	18.62

ODISE [39] and CAT-Seg [8]. As shown, all models perform well on larger objects but focus on different smaller objects. Then we use the generated pseudo-labeled ground truth to train the OVO networks, with the results listed in Table 5. The networks achieve comparable performance with different segmentation models. In this work, we use SAN [40] for fair comparison with previous approaches.

Language Autoencoder. We conduct experiments to verify the effectiveness of the autoencoder. Without it, the model is required to generate 3D features with a dimension of 512. In this case, we set the voxel feature dimension after the 2D-to-3D transformation for BEVDet [12] and BEVDet4D [11] to 128. For BEVFormer [20], the BEV queries are kept at a dimension of 256, as using a larger dimension exceeds the GPU memory. As shown in Table 6, introducing autoencoder can effectively reduce the memory requirements with better performance. Here, we hypothesize that this is because CLIP model is trained using 400 million (image, text) pairs, thus its high-dimensional space could be highly compact. Instead, the number of extracted texts is around one thousand in this work, which is significantly smaller than the number of texts used in CLIP training, resulting a sparse space and allowing us to further compress it.

Table 6. Ablation study on the language autoencoder.

Method	w/o autoencoder			w/ autoencoder		
	mIoU \uparrow	Memory (G) \downarrow	Params (M) \downarrow	mIoU \uparrow	Memory (G) \downarrow	Params \downarrow
LOcc-BEVFormer	17.36	1.41	61.80	18.62	1.18	61.70
LOcc-BEVDet	20.25	2.22	92.40	20.29	1.11	41.60
LOcc-BEVDet4D	22.62	2.33	100.00	22.68	1.11	48.00

4.5. Qualitative Results

Fig. 6 presents visualizations of the pseudo-labeled ground truth, along with results from LOcc-BEVFormer, LOcc-BEVDet, and LOcc-BEVDet4D trained on it. Each model demonstrates clear predictions, despite the noise present in the training dataset. This demonstrates the ability of the models to learn useful information from semi-labeled data. These findings are also observed in other vision tasks, such as image segmentation [16], video segmentation [29], and depth estimation [41].

5. Conclusions

In this paper, we have presented LOcc, an effective and generalizable framework for open-vocabulary occupancy prediction. We propose a semantic transitive labeling pipeline for generating dense and fine-grained 3D language occupancy ground truth. We experimentally demonstrate that text semantic labels can be effectively transferred from images to LiDAR point clouds and ultimately to voxels, diminishing labor-intensive human annotations. By replacing the original prediction head with a geometry head and a language head, LOcc is compatible with most existing supervised networks. Based on the BEVFormer, BEVDet, and BEVDet4D, our proposed method can achieve better results than all the previous state-of-the-art zero-shot occupancy prediction methods.

References

- [1] Jinze Bai, Shuai Bai, Yunfei Chu, Zeyu Cui, Kai Dang, Xiaodong Deng, Yang Fan, and et al. Qwen technical report. *arXiv preprint arXiv:2309.16609*, 2023. 2, 3
- [2] Jinze Bai, Shuai Bai, Shusheng Yang, Shijie Wang, Sinan Tan, Peng Wang, Junyang Lin, Chang Zhou, and Jingren Zhou. Qwen-vl: A versatile vision-language model for understanding, localization, text reading, and beyond. *arXiv preprint arXiv:2308.12966*, 2023. 2, 3, 4
- [3] Jens Behley, Martin Garbade, Andres Milioto, Jan Quenzel, Sven Behnke, Cyrill Stachniss, and Jürgen Gall. Semantickitti: A dataset for semantic scene understanding of lidar sequences. In *Proceedings of the IEEE/CVF International Conference on Computer Vision*, pages 9297–9307, 2019. 2
- [4] Simon Boeder, Fabian Gigengack, and Benjamin Risse. Langocc: Self-supervised open vocabulary occupancy estimation via volume rendering. *arXiv preprint arXiv:2407.17310*, 2024. 2
- [5] Holger Caesar, Varun Bankiti, Alex H Lang, Sourabh Vora, Venice Erin Liong, Qiang Xu, Anush Krishnan, Yu Pan, Giancarlo Baldan, and Oscar Beijbom. nuscenes: A multi-modal dataset for autonomous driving. In *Proceedings of the IEEE/CVF Conference on Computer Vision and Pattern Recognition*, pages 11621–11631, 2020. 6
- [6] Anh-Quan Cao and Raoul De Charette. Monoscene: Monocular 3d semantic scene completion. In *Proceedings of the IEEE/CVF Conference on Computer Vision and Pattern Recognition*, pages 3991–4001, 2022. 2, 6
- [7] Tianheng Cheng, Lin Song, Yixiao Ge, Wenyu Liu, Xinggang Wang, and Ying Shan. Yolo-world: Real-time open-vocabulary object detection. In *Proceedings of the IEEE/CVF Conference on Computer Vision and Pattern Recognition*, pages 16901–16911, 2024. 3
- [8] Seokju Cho, Heeseong Shin, Sunghwan Hong, Anurag Arnab, Paul Hongsuck Seo, and Seungryong Kim. Catseg: Cost aggregation for open-vocabulary semantic segmentation. In *Proceedings of the IEEE/CVF Conference on Computer Vision and Pattern Recognition*, pages 4113–4123, 2024. 2, 3, 4, 8
- [9] Kaiming He, Xiangyu Zhang, Shaoqing Ren, and Jian Sun. Deep residual learning for image recognition. In *Proceedings of the IEEE Conference on Computer Vision and Pattern Recognition*, pages 770–778, 2016. 5, 6
- [10] Yihan Hu, Jiazhi Yang, Li Chen, Keyu Li, Chonghao Sima, Xizhou Zhu, Siqi Chai, Senyao Du, Tianwei Lin, Wenhai Wang, et al. Planning-oriented autonomous driving. In *Proceedings of the IEEE/CVF Conference on Computer Vision and Pattern Recognition*, pages 17853–17862, 2023. 1
- [11] Junjie Huang and Guan Huang. Bevdet4d: Exploit temporal cues in multi-camera 3d object detection. *arXiv preprint arXiv:2203.17054*, 2022. 2, 5, 6, 8
- [12] Junjie Huang, Guan Huang, Zheng Zhu, Yun Ye, and Dalong Du. Bevdet: High-performance multi-camera 3d object detection in bird-eye-view. *arXiv preprint arXiv:2112.11790*, 2021. 2, 5, 6, 8
- [13] Yuanhui Huang, Wenzhao Zheng, Yunpeng Zhang, Jie Zhou, and Jiwen Lu. Tri-perspective view for vision-based 3d semantic occupancy prediction. In *Proceedings of the IEEE/CVF Conference on Computer Vision and Pattern Recognition*, pages 9223–9232, 2023. 2, 6
- [14] Yuanhui Huang, Wenzhao Zheng, Borui Zhang, Jie Zhou, and Jiwen Lu. Selfocc: Self-supervised vision-based 3d occupancy prediction. In *Proceedings of the IEEE/CVF Conference on Computer Vision and Pattern Recognition*, pages 19946–19956, 2024. 6
- [15] Justin Kerr, Chung Min Kim, Ken Goldberg, Angjoo Kanazawa, and Matthew Tancik. Lrf: Language embedded radiance fields. In *Proceedings of the IEEE/CVF International Conference on Computer Vision*, pages 19729–19739, 2023. 3
- [16] Alexander Kirillov, Eric Mintun, Nikhila Ravi, Hanzi Mao, Chloe Rolland, Laura Gustafson, Tete Xiao, Spencer Whitehead, Alexander C Berg, Wan-Yen Lo, et al. Segment anything. In *Proceedings of the IEEE/CVF International Conference on Computer Vision*, pages 4015–4026, 2023. 3, 8
- [17] Boyi Li, Kilian Q Weinberger, Serge Belongie, Vladlen Koltun, and Rene Ranftl. Language-driven semantic segmentation. In *International Conference on Learning Representations*, 2023. 2, 3
- [18] Siyuan Li, Tobias Fischer, Lei Ke, Henghui Ding, Martin Danelljan, and Fisher Yu. Ovtrack: Open-vocabulary multiple object tracking. In *Proceedings of the IEEE/CVF conference on computer vision and pattern recognition*, pages 5567–5577, 2023. 3
- [19] Yiming Li, Zhiding Yu, Christopher B. Choy, Chaowei Xiao, José M. Álvarez, Sanja Fidler, Chen Feng, and Anima Anandkumar. Voxformer: Sparse voxel transformer for camera-based 3d semantic scene completion. In *Proceedings of the IEEE/CVF Conference on Computer Vision and Pattern Recognition*, pages 9087–9098, 2023. 2
- [20] Zhiqi Li, Wenhai Wang, Hongyang Li, Enze Xie, Chonghao Sima, Tong Lu, Yu Qiao, and Jifeng Dai. Bevformer: Learning bird’s-eye-view representation from multi-camera images via spatiotemporal transformers. In *Proceedings of the European Conference on Computer Vision*, pages 1–18, 2022. 1, 2, 5, 6, 8
- [21] Haotian Liu, Chunyuan Li, Qingyang Wu, and Yong Jae Lee. Visual instruction tuning. *Advances in Neural Information Processing Systems*, 36, 2024. 2, 3
- [22] I Loshchilov. Decoupled weight decay regularization. *arXiv preprint arXiv:1711.05101*, 2017. 6
- [23] Qihang Ma, Xin Tan, Yanyun Qu, Lizhuang Ma, Zhizhong Zhang, and Yuan Xie. Cotr: Compact occupancy transformer for vision-based 3d occupancy prediction. *arXiv preprint arXiv:2312.01919*, 2023. 2
- [24] Mingjie Pan, Jiaming Liu, Renrui Zhang, Peixiang Huang, Xiaoqi Li, Hongwei Xie, Bing Wang, Li Liu, and Shanghang Zhang. Renderocc: Vision-centric 3d occupancy prediction with 2d rendering supervision. In *IEEE International Conference on Robotics and Automation*, pages 12404–12411, 2024. 1
- [25] Songyou Peng, Kyle Genova, Chiyu Jiang, Andrea Tagliasacchi, Marc Pollefeys, Thomas Funkhouser, et al.

- Openscene: 3d scene understanding with open vocabularies. In *Proceedings of the IEEE/CVF Conference on Computer Vision and Pattern Recognition*, pages 815–824, 2023. 3
- [26] Jonah Philion and Sanja Fidler. Lift, splat, shoot: Encoding images from arbitrary camera rigs by implicitly unprojecting to 3d. In *Proceedings of the European Conference on Computer Vision*, pages 194–210, 2020. 5
- [27] Minghan Qin, Wanhua Li, Jiawei Zhou, Haoqian Wang, and Hanspeter Pfister. Langsplat: 3d language gaussian splatting. In *Proceedings of the IEEE/CVF Conference on Computer Vision and Pattern Recognition*, pages 20051–20060, 2024. 3
- [28] Alec Radford, Jong Wook Kim, Chris Hallacy, Aditya Ramesh, Gabriel Goh, Sandhini Agarwal, Girish Sastry, Amanda Askell, Pamela Mishkin, Jack Clark, et al. Learning transferable visual models from natural language supervision. In *Proceedings of the International Conference on Machine Learning*, pages 8748–8763, 2021. 2, 3
- [29] Nikhila Ravi, Valentin Gabeur, Yuan-Ting Hu, Ronghang Hu, Chaitanya Ryali, Tengyu Ma, Haitham Khedr, Roman Rädle, Chloe Rolland, Laura Gustafson, et al. Sam 2: Segment anything in images and videos. *arXiv preprint arXiv:2408.00714*, 2024. 8
- [30] Xiaoyu Tian, Tao Jiang, Longfei Yun, Yucheng Mao, Huitong Yang, Yue Wang, Yilun Wang, and Hang Zhao. Occ3d: A large-scale 3d occupancy prediction benchmark for autonomous driving. In *Advances in Neural Information Processing Systems*, pages 64318–64330, 2023. 1, 2, 6, 8
- [31] Wenwen Tong, Chonghao Sima, Tai Wang, Li Chen, Silei Wu, Hanming Deng, Yi Gu, Lewei Lu, Ping Luo, Dahua Lin, et al. Scene as occupancy. In *Proceedings of the IEEE/CVF International Conference on Computer Vision*, pages 8406–8415, 2023. 1, 2
- [32] Antonin Vobecky, Oriane Siméoni, David Hurych, Spyridon Gidaris, Andrei Bursuc, Patrick Pérez, and Josef Sivic. Pop-3d: Open-vocabulary 3d occupancy prediction from images. In *Advances in Neural Information Processing Systems*, 2024. 1, 2, 3
- [33] Tai Wang, Xiaohan Mao, Chenming Zhu, Runsen Xu, Ruiyuan Lyu, Peisen Li, Xiao Chen, Wenwei Zhang, Kai Chen, Tianfan Xue, et al. Embodiedscan: A holistic multi-modal 3d perception suite towards embodied ai. In *Proceedings of the IEEE/CVF Conference on Computer Vision and Pattern Recognition*, pages 19757–19767, 2024. 1
- [34] Xiaofeng Wang, Zheng Zhu, Wenbo Xu, Yunpeng Zhang, Yi Wei, Xu Chi, Yun Ye, Dalong Du, Jiwen Lu, and Xingang Wang. Openoccupancy: A large scale benchmark for surrounding semantic occupancy perception. In *Proceedings of the IEEE/CVF International Conference on Computer Vision*, pages 17850–17859, 2023. 1, 2
- [35] Jason Wei, Xuezhi Wang, Dale Schuurmans, Maarten Bosma, Fei Xia, Ed Chi, Quoc V Le, Denny Zhou, et al. Chain-of-thought prompting elicits reasoning in large language models. *Advances in Neural Information Processing Systems*, 35:24824–24837, 2022. 3
- [36] Yi Wei, Linqing Zhao, Wenzhao Zheng, Zheng Zhu, Jie Zhou, and Jiwen Lu. Surroundocc: Multi-camera 3d occupancy prediction for autonomous driving. In *Proceedings of the IEEE/CVF International Conference on Computer Vision*, pages 21729–21740, 2023. 1, 2
- [37] Yuan Wu, Zhiqiang Yan, Zhengxue Wang, Xiang Li, Le Hui, and Jian Yang. Deep height decoupling for precise vision-based 3d occupancy prediction. *arXiv preprint arXiv:2409.07972*, 2024. 2
- [38] Huaiyuan Xu, Junliang Chen, Shiyu Meng, Yi Wang, and Lap-Pui Chau. A survey on occupancy perception for autonomous driving: The information fusion perspective. *arXiv preprint arXiv:2405.05173*, 2024. 1
- [39] Jiarui Xu, Sifei Liu, Arash Vahdat, Wonmin Byeon, Xiaolong Wang, and Shalini De Mello. Open-vocabulary panoptic segmentation with text-to-image diffusion models. In *Proceedings of the IEEE/CVF Conference on Computer Vision and Pattern Recognition*, pages 2955–2966, 2023. 2, 3, 8
- [40] Mengde Xu, Zheng Zhang, Fangyun Wei, Han Hu, and Xiang Bai. Side adapter network for open-vocabulary semantic segmentation. In *Proceedings of the IEEE/CVF Conference on Computer Vision and Pattern Recognition*, pages 2945–2954, 2023. 2, 3, 7, 8
- [41] Lihe Yang, Bingyi Kang, Zilong Huang, Xiaogang Xu, Jiashi Feng, and Hengshuang Zhao. Depth anything: Unleashing the power of large-scale unlabeled data. In *Proceedings of the IEEE/CVF Conference on Computer Vision and Pattern Recognition*, pages 10371–10381, 2024. 8
- [42] Zhangchen Ye, Tao Jiang, Chenfeng Xu, Yiming Li, and Hang Zhao. Cvt-occ: Cost volume temporal fusion for 3d occupancy prediction. *arXiv preprint arXiv:2409.13430*, 2024. 2, 6
- [43] Zhu Yu, Runmin Zhang, Jiacheng Ying, Junchen Yu, Xiaohai Hu, Lun Luo, Si-Yuan Cao, and Hui-Liang Shen. Context and geometry aware voxel transformer for semantic scene completion. In *Advances in Neural Information Processing Systems*, 2024. 2
- [44] Alireza Zareian, Kevin Dela Rosa, Derek Hao Hu, and Shih-Fu Chang. Open-vocabulary object detection using captions. In *Proceedings of the IEEE/CVF Conference on Computer Vision and Pattern Recognition*, pages 14393–14402, 2021. 3
- [45] Chubin Zhang, Juncheng Yan, Yi Wei, Jiaxin Li, Li Liu, Yansong Tang, Yueqi Duan, and Jiwen Lu. Occnerf: Self-supervised multi-camera occupancy prediction with neural radiance fields. *arXiv preprint arXiv:2312.09243*, 2023. 6
- [46] Yunpeng Zhang, Zheng Zhu, and Dalong Du. Occformer: Dual-path transformer for vision-based 3d semantic occupancy prediction. In *Proceedings of the IEEE/CVF International Conference on Computer Vision*, pages 9433–9443, 2023. 2, 6
- [47] Jilai Zheng, Pin Tang, Zhongdao Wang, Guoqing Wang, Xiangxuan Ren, Bailan Feng, and Chao Ma. Veon: Vocabulary-enhanced occupancy prediction. *arXiv preprint arXiv:2407.12294*, 2024. 1, 2, 3, 6
- [48] Yupeng Zheng, Xiang Li, Pengfei Li, Yuhang Zheng, Bu Jin, Chengliang Zhong, Xiaoxiao Long, Hao Zhao, and Qichao Zhang. Monoocc: Digging into monocular semantic occupancy prediction. *arXiv preprint arXiv:2403.08766*, 2024. 2